

Pressure-stabilized superconducting electride Li_5C

Qinfang Wang,¹ Wenwen Cui^{1,*}, Kun Gao,¹ Ju Chen,² Tingting Gu¹, Meixu Liu,¹ Jian Hao,¹
Jingming Shi¹, and Yinwei Li^{1,3,†}

¹Laboratory of Quantum Functional Materials Design and Application, School of Physics and Electronic Engineering,
Jiangsu Normal University, Xuzhou 221116, China

²Department of Physics, School of Physics and Electronic Science, East China Normal University, Shanghai 200241, China

³Shandong Key Laboratory of Optical Communication Science and Technology, School of Physical Science & Information Technology
of Liaocheng University, Liaocheng 252059, China



(Received 27 June 2022; revised 9 August 2022; accepted 17 August 2022; published 29 August 2022)

The search for electrides has recently attracted great interest owing to their unique physical properties, such as superconductivity. Li_5C has been proposed as a candidate electride with a high superconducting critical temperature T_c of 48 K originating mainly from the localized electrons. Here, a combination of structure searches and first-principles calculations has been performed to acquire the phase diagrams of a Li-C system at high pressure. The structure searches unraveled four successive structures under pressure for Li_5C that are energetically more stable than the previously proposed superconducting one. The dimension of the localized electrons in Li_5C decreases under compression due to the reduced interstitial voids. Electron-phonon calculations demonstrated that the four Li_5C phases are superconductors with a maximum T_c of 5.7 K, excluding its possibility of high superconductivity. Analysis showed that the host hybridized electrons, instead of interstitial electrons, contribute mainly to the superconductivity in Li_5C .

DOI: [10.1103/PhysRevB.106.054519](https://doi.org/10.1103/PhysRevB.106.054519)

I. INTRODUCTION

Electrides are special ionic compounds in which interstitial quasiatoms (ISQs) behave as anions [1–3]. The organic electride $\text{Cs}^+(\text{I8C6})_2:(e^-)$ was the first electride to be synthesized experimentally [4]; however, the practical applications of organic electrides are greatly restricted by their instability above room temperature and chemical sensitivity to air and moisture [1]. The discovery of the first stable inorganic electride, $[\text{Ca}_{24}\text{Al}_{28}\text{O}_{64}]^{4+}(4e^-)$ (C12A7: e^-), which is much more stable [5], has opened up applications for electrides including catalysis [6], electronics [7], and batteries [8].

According to ISQ topologies, electrides are categorized as zero dimensional (0D; cavities) [5,9], one dimensional (1D; linked) [10], two dimensional (2D) [7,11], or three dimensional (3D) [12,13]. Electron conductivity is closely related to its dimensional characteristics. Low-dimensional 0D electrides usually exhibit poor conductivity owing to the cavities confining electrons, whereas high-dimensional electrides are likely to allow electron conduction because of the delocalization of the anionic electrons [3,14]. For example, the 0D electride $hP4$ Na shows insulating behavior with a large band gap [9], and transforms to a 3D metallic electride $cI24$ structure, where the ISQs form a conducting channels [13].

Electrides are prone to be insulating because of the strong localization of both interstitial and orbital electrons [9,15,16]. Exceptionally, some electrides, such as C12A7: e^-

[17], Mn_5Si_3 -type Nb_5Ir_3 [18], and Zr_5Sb_3 [19], are experimentally observed to exhibit metallic properties, and even possess superconductivity with a T_c of 0.4, 9.4, and 2.3 K at ambient pressure, respectively. Thus, superconducting electrides are now a new category of superconductors that have attracted intense interest [17]. Nevertheless, only a few electrides exist at ambient pressure, which significantly limits their further applications, despite high pressure being an effective method to stabilize new materials with exotic properties. Indeed, the inorganic electride family has been greatly enriched by the discovery of high-pressure electrides [9,13,20–29]. As pressure increases, the energies of the valence orbitals of atoms increase more rapidly than those of the ISQs, which results in electrons moving to the interstitial space [30]. Various electrides are stabilized under high pressure, including elements [9,13,20] and compounds [21–28]. In addition, high pressure can improve the superconductivity of electrides. For example, the T_c of C12A7: e^- increases from 0.2 K at ambient pressure to 1.79 K at 4.7 GPa [31], and Li_6P is predicted to be a good superconductor with a high T_c of 39.3 K at 270 GPa [24]. By far, there are two distinctively different standpoints to elucidate the superconducting mechanism of electrides: (i) ISQ-derived superconductivity, e.g., Li_6P [24] and C12A7: e^- [17]; (ii) low ISQ concentration favors good superconductivity, e.g., Nb_5Ir_3 [18] and Li_5Si [28].

Electrides are easier to be discovered among lithium compounds [21–28] because Li has a relatively incompressible core, in which s valence electrons relocate more readily to interstitial areas. C, which has a moderate electronegativity (2.55), is an ideal element for attracting electrons to populate separate interstitial orbitals, instead of binding electrons to

*wenwencui@jsnu.edu.cn

†yinwei_li@jsnu.edu.cn

anions. Therefore, lithium carbides are promising candidates for electrides. Previous research has identified a series of lithium carbides (e.g., LiC_{12} [32,33], Li_2C_2 [34–37], Li_2C_3 [38], Li_4C [39], Li_5C [40], and Li_6C [41]); among these, Li_6C [41] and Li_5C [40] have been predicted to be good superconducting electrides with a T_c of 10 and 48 K at high pressure, respectively.

Here, in order to obtain the complete phase diagram of a Li-C system, we investigate the crystal structures of various stoichiometric Li_xC_y compounds under high pressures up to 200 GPa. We found that Li_5C is a superconducting electride with a maximum T_c of 5.7 K, which is much lower than the previously predicted 48 K [40]. Additionally, Li_6C is demonstrated to be an insulator at high pressure. Our results alter the previous perspective about structures and properties of the Li-C system and stress the need for a thorough search for a crystalline ground state.

II. COMPUTATIONAL DETAILS

To search for thermodynamically stable Li_xC_y candidate compounds under pressure, a structural prediction was performed using the swarm intelligence-based crystal structure analysis by particle swarm optimization (CALYPSO) program [42–45], which has successfully predicted several metastable and stable compounds [46–49]. The predictions of the crystal structures of Li_xC_y ($x, y = 1\text{--}6$) were performed at 50, 100, and 200 GPa. The maximum number of atoms in the simulation cell for each composition was no more than 28. In order to find the ground state of Li-C compounds during the prediction, more than 2000 structures were sampled for each prediction run and the structural search was considered converged when ~ 1000 structures were generated after finding the lowest-energy structure. In each structure prediction, 60% of the structures with lower enthalpies were selected to build next-generation structures by particle swarm optimization, and 40% of the structures in the new generation were randomly generated. These procedures greatly increase the diversity of the structures, which is crucial for structural global search efficiency. Structural relaxations and electronic structure calculations were performed using the projector augmented-wave (PAW) method, as implemented in the Vienna *ab initio* simulation package (VASP) [50]. The density functional theory exchange-correlation functional was approximated by the Perdew-Burke-Ernzerhof (PBE) generalized gradient approximation [51]. The all-electron PAW method was used for Li and C atoms with valence configurations of $1s^2 2s^1$ and $2s^2 2p^2$, respectively. The cutoff energy for the expansion of the wave function in the plane-wave basis was set to 1000 eV. Monkhorst-Pack k -point meshes [52] with a grid density of 0.20 \AA^{-1} were chosen to ensure a total energy convergence of better than 1 meV per atom. The single-point energy calculations using the Heyd-Scuseria-Ernzerhof (HSE06) hybrid functional [53] were also performed to estimate the band gap. Finally, the optB88-vdW van der Waals density functional was used to include dispersion in the exchange-correlation functionals [54] for all the optimizations. The dynamical stability was determined by calculating phonon frequencies using the supercell finite displacement method [55] within the PHONOPY code [56].

Electron-phonon coupling (EPC) calculations were conducted with the density functional perturbation (linear response) theory, as implemented in the QUANTUM ESPRESSO package [57]. Ultrasoft pseudopotentials for the Li and C elements were used with a kinetic energy cutoff of 80 Ry. The T_c values of all metallic Li_xC_y compounds were estimated with the Allen-Dynes modified McMillan formula [58].

III. RESULTS AND DISCUSSION

To investigate the phase stability of Li-C systems, we calculated the formation enthalpies of all considered Li-C compositions with respect to decomposition into elementary substances to construct the convex hulls, as shown in Figs. 1(a)–1(c). There are eight energetically stable Li_xC_y compounds, shown by solid squares on the convex hulls, for which we calculated the relative enthalpies with respect to other Li_xC_y compounds or elements as functions of pressure to obtain the phase diagrams [Fig. 1(d)]. The vdW interaction has proved to be important for predictions of both structural and energetic information for graphite and graphite intercalated lithium compounds [38,59]. Given that both Li_2C_3 and LiC_2 contain graphene sublattices, we consider the vdW interaction for all the Li-C compounds during the structural relaxation [please see Supplemental Material (SM) [60] Fig. S1]. In addition to the previously observed or proposed structures (shaded gray bars), we identified nine different stable structures [colored bars, Fig. 1(d)], namely the $Cmmm$ and the $P1$ structure for Li_6C ; the $P\bar{3}m1$, the $Cmcm$ -I, the $C2/m$, and the $Cmcm$ -II structures for Li_5C ; the $R\bar{3}m$ structure for Li_3C ; and the $C2/m$ and the $P\bar{1}$ structures for Li_2C . All of the stable phases are dynamically stable with no negative frequencies (Fig. S2 in SM [60]). Moreover, we found that the carbon motifs in the Li-C compounds evolved in the following sequence with increasing carbon content (Table I and Fig. S3): isolated C anions (Li_6C , Li_5C , and Li_4C); a mixture of isolated C anions and C_2 dimers (Li_3C); C_2 dimers and C_4 zigzag tetramers (Li_2C); single carbon ribbons (Li_3C_4); double carbon ribbons (Li_2C_3); and graphene (LiC_2). Li_5C and Li_6C are typical electrides; however, Li_6C is insulating under high pressure (Figs. S4 and S5). Note that Li_6C is previously reported with a T_c of 10 K (80 GPa in the $R\bar{3}m$ structure). However, the superconductivity in Li_6C is suppressed when transforming to the $Cmmm$ phase (47 GPa) and even becomes a semiconductor in the $P1$ phase (Fig. S5). We also investigate the superconductivity of other metallic lithium carbides as summarized in Table II. Except Li_5C , all of them exhibit very weak superconductivity (< 1 K) under high pressure, thus hereafter, our calculations and discussions will focus on the Li_5C .

Under compression, Li_5C exhibits complicated phase transitions [Fig. 1(d)]. The hexagonal $P\bar{3}m1$ structure became stable at 42 GPa. In this structure each C atom is coordinated with 14 Li atoms, forming a CLi_{14} octadecahedron [Fig. 2(a)], with an average Li-C distance of 2.13 Å at 50 GPa. Two CLi_{14} polyhedrons are connected with each other by face sharing. As pressure increases, an orthorhombic $Cmcm$ -I structure emerges at 53 GPa, also consisting of CLi_{14} polyhedrons [Fig. 2(b)]. The two centered CLi_{14} are linked by face sharing and then connected to the ones in the corner via edge

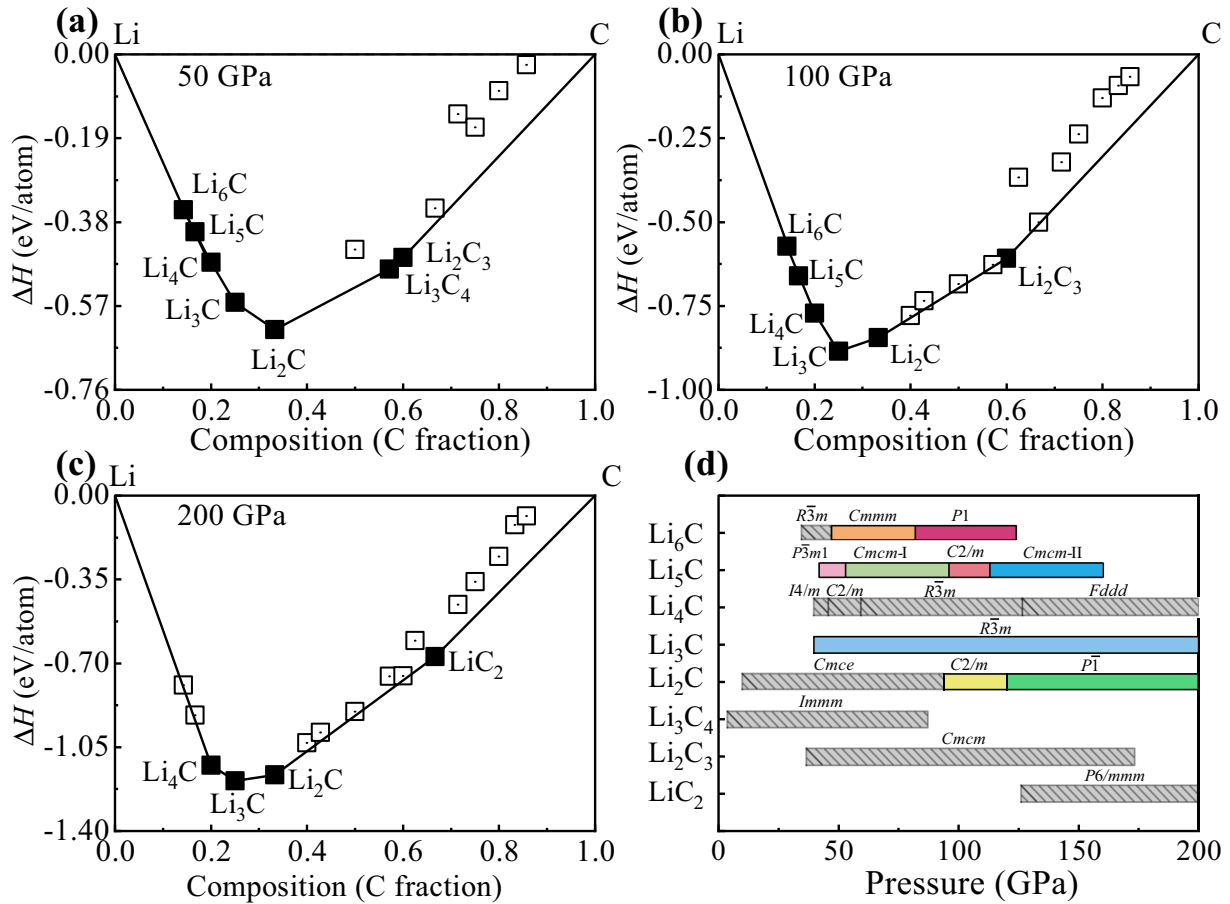


FIG. 1. Thermodynamic stabilities and stable pressure ranges of Li_xC_y compounds. (a)–(c) Formation enthalpies (ΔH) per atom of the Li_xC_y compounds at 50, 100, and 200 GPa, respectively. (d) Pressure-composition phase diagram for all stable Li_xC_y compounds, where gray areas denote previously reported structures and colored areas our predicted structures. The detailed enthalpies for each compound as a function of pressure are shown in Fig. S1.

sharing. Then it transforms to the $C2/m$ structure [Fig. 2(c)] at 96 GPa, and finally another orthorhombic $Cmcm$ structure at 113 GPa, denoted as the $Cmcm-II$ phase [Fig. 2(d)]. Under high pressure, the coordination environment of the C atoms in Li_5C does not change greatly, and the structures are composed of CLi_{14} units, except $Cmcm-II$, which is composed of CLi_{15}

units due to the extreme compression. All of the Li-C bonds in Li_5C exhibit ionic characters, confirmed by the Bader charge analysis (Table S1). We have also predicted the previously reported $P6/mmm$ with a T_c of 48 K [40], however, unexpectedly, it possesses a much higher enthalpy (e.g., 0.91 eV per f.u. at 200 GPa) than that of our four predicted phases, and thus

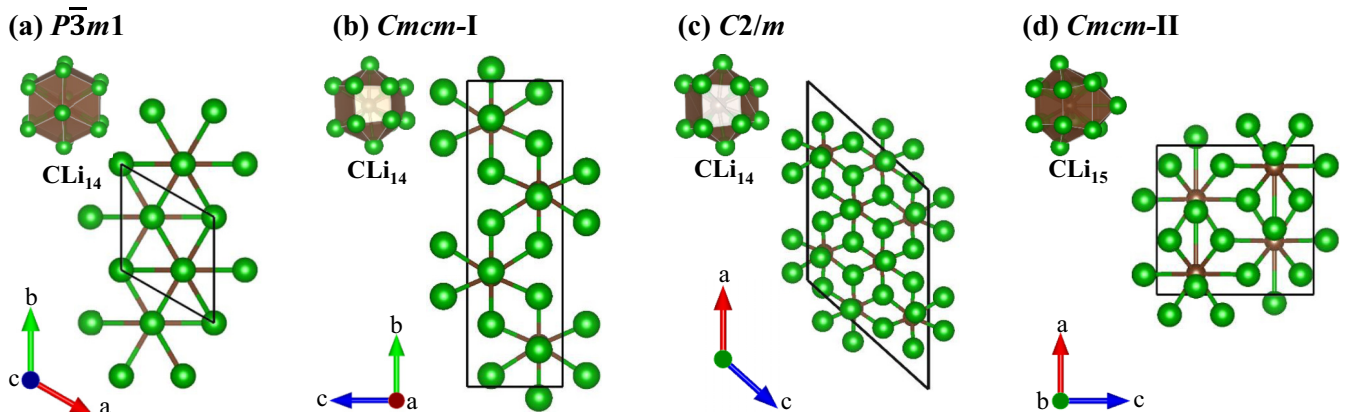


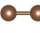
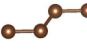
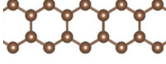
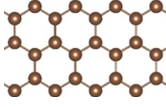
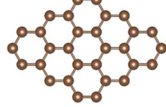


FIG. 2. Crystal structures of Li_5C at high pressures. (a) $P3m1$ at 50 GPa, (b) $Cmcm-I$ at 60 GPa, (c) $C2/m$ at 100 GPa, and (d) $Cmcm-II$ at 120 GPa. Green and brown spheres represent Li and C atoms, respectively.

TABLE I. Carbon motifs in the pressure-induced stable Li-C compounds.

Li_xC_y	Pressure (GPa)	C motifs
$\text{Li}_{4,5,6}\text{C}$	35–200	
Li_3C	40–200	
Li_2C	10–120	
	120–200	
Li_3C_4	4–87	
Li_2C_3	37–173	
LiC_2	127–200	

the previous structure is energetically unstable over the whole range [Fig. S1(b)]. The reason for the discrepancy in the predictions is probably due to the complexity of the ground state of Li_5C , indicating that more structures and repeated simulations are required in the prediction run, especially for those stoichiometries containing a large number of atoms in the unit cell (e.g., $N > 20$).

According to the octet rule, Li_5C can be represented theoretically as $(\text{Li}_5\text{C})^+(e^-)$, and the excess of electrons leads to the formation of electrides, as shown by the electron lo-

TABLE II. The calculated electron phonon coupling parameter (λ), logarithmic average phonon frequency (ω_{\log}), and the estimated T_c for selected Li_xC_y structures using the Allen-Dynes modified McMillan (ADM) equation with $\mu^* = 0.10$.

Li_xC_y	Phase	Pressure (GPa)	λ	ω_{\log} (K)	T_c (K)
Li_6C	<i>Cmmm</i>	50	0.23	659	0.01
Li_5C	<i>P3m1</i>	50	0.38	478	1.5
	<i>Cmcm-I</i>	95	0.49	503	5.7
	<i>C2/m</i>	100	0.44	470	3.1
	<i>Cmcm-II</i>	120	0.41	660	3.1
		140	0.42	671	3.6
		160	0.43	673	4.3
Li_2C	<i>Cmce</i>	50	0.2	666	0.09
	<i>C2/m</i>	100	0.24	782	0.02
Li_3C_4	<i>Immm</i>	50	0.25	1084	0.06
LiC_2	<i>P6/mmm</i>	100	0.24	1279	0.4

calization function (ELF; Fig. 3). The presence of interstitial confined electrons was confirmed by the partial charge densities (Fig. S6). In *P3m1*, the ISQs are dispersed loosely in the interlayer spaces to form 2D electrides in the (001) plane [Fig. 3(a)]. In the *Cmcm-I* phase [Fig. 3(b)], there are infinite 1D zigzag chains of ISQs inside the channels, formed by face-sharing CLi_{14} along the *c* axis. In the *C2/m* phase, the ISQs are rearranged into an hourglass-shaped distribution at the vertices of the monoclinic lattice [Fig. 3(c)]. Further compression-induced ISQs that are more localized and have a lozenge shape along the *a* axis in the *Cmcm-II* phase [Fig. 3(d)]. The dimensionality reduction of the electrides is consistent with the Bader charge analysis (Table S1), in which the ISQs in Li_5C become smaller with increasing pressure, i.e., 0.76, 0.68, 0.49, and 0.43e for *P3m1*, *Cmcm-I*, *C2/m*, and *Cmcm-II*, respectively.

The band structures and partial densities of state (DOS) for Li_5C were calculated to explore the electronic properties further [Figs. 4(a) and S7]. Upon compression, all the Li_5C structures remain metallic with a large contribution from Li-*p* electrons as well as strong hybridization between the ISQs and atomic orbital electrons (C-*p* and Li-*p*) at the Fermi level (E_f). Owing to the metallic character of Li_5C , the EPC was calculated to estimate the potential superconductivity. The EPC parameters (λ) are 0.38, 0.49, 0.44, and 0.41 for *P3m1* at 50 GPa, *Cmcm-I* at 95 GPa, *C2/m* at 100 GPa, and *Cmcm-II* at 120 GPa, respectively (Table II). The T_c values were estimated using the Allen-Dynes modified McMillan equation [58], using a typical Coulomb pseudopotential of $\mu^* = 0.1$. Accordingly, the estimated T_c values are 1.5, 5.7, 3.1, and 3.1 K for the *P3m1*, *Cmcm-I*, *C2/m*, and *Cmcm-II* phases, respectively. The relatively higher superconductivity of *Cmcm-I* is attributed to the higher occupation of the total DOS [Fig. 4(a)] at E_f and stronger EPC among Li_5C structures. Next, we will focus on investigating the pressure-dependent superconductivity of this phase.

The phonon dispersions, projected phonon DOS, Eliashberg spectral function α^2F , and EPC integral $\lambda(\omega)$ for *Cmcm-I* were calculated [Figs. 4(b) and 4(c)]. *Cmcm-I* has a relatively large λ of 0.49 at 95 GPa, comparable to that of Li_6C at 40 GPa (0.47) [41] and larger than that of Li_4C at 50 GPa (0.276) [39]. According to the EPC integral, the low frequencies (below 14 THz) make the main contribution to the total λ (~69%). To investigate the pressure dependence of the superconductivity of *Cmcm-I*, we calculated its T_c under different pressures [Fig. 4(c)]. λ increases with pressure, whereas the DOS at E_f , denoted as $N(E_f)$, decrease, which mainly originates from the decrease of ISQs at E_f [Fig. 4(c)] and has small coupling with the vibration due to the confined electrons in the 1D channel. Thus, even if $N(E_f)$ slightly decreases, the proportion of free electrons from Li/C does not. λ is proportional to the proportion of the total number of free electrons in $N(E_f)$ that has coupling with the phonons and is inversely proportional to the total number of ISQs. The DOS at E_f of *Cmcm-I* consists of the hybridization of ISQs with Li-*p* and C-*p* orbital electrons [Fig. 4(a)], whereas the number of ISQs decreases with pressure; thus, the increase in λ is attributed to the interaction between the hybridized states of the host Li-*p* and C-*p* orbitals with the phonons. The

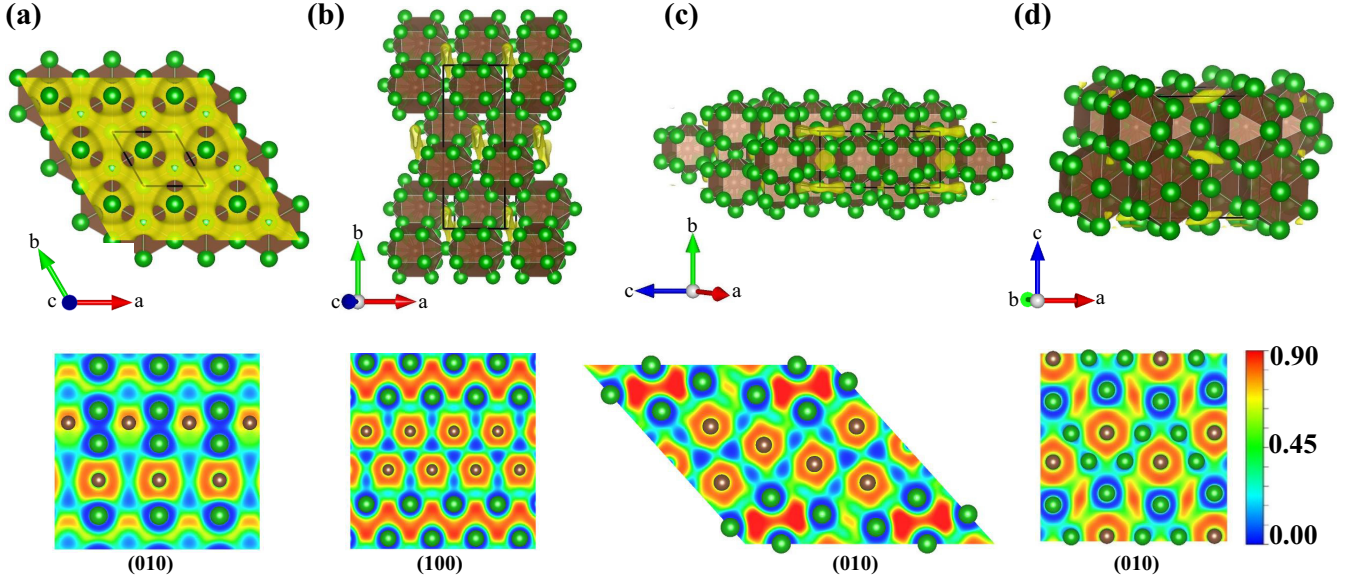


FIG. 3. 3D (top panel) and 2D (bottom panel) ELF maps of Li_5C compounds. (a) $P\bar{3}m1$ at 50 GPa, (b) $Cmcm-I$ at 95 GPa, (c) $C2/m$ at 100 GPa, and (d) $Cmcm-II$ at 120 GPa. The 3D ELF maps have isosurface values of 0.55, 0.7, 0.7, and 0.7, respectively.

increase in λ enhances T_c for $Cmcm-I$ from 3.7 K at 60 GPa to 5.7 K at 95 GPa, which is larger than the highest value of T_c (4.7 K) for Li_4C [39], as well as that for other typical electride superconductors (e.g., C12A7:e^- , 0.4 K [17]; Zr_5Sb_3 , 2.3 K [19]; MgONa , 3.4 K [61]; Y_2C , 0.9 K [61]; and Ca_2N , 4.7 K [62]). We should emphasize that the T_c of the $Cmcm-I$ phase is much smaller than that of the $P6/mmm$ structure (~ 48 K at 210 GPa), whose superconductivity originates mainly from the high conductivity of 2D ISQ topology with a large occupation at E_f [40], however, it is not stable over the whole pressure range. The superior superconductivity of $P6/mmm$ is not unreasonable, considering its larger DOS at E_f (~ 1.50 eV^{-1} per f.u.) and stronger electron-coupling parameter λ (1.26) [40] compared with that of the $Cmcm-I$ structure. Thus, a key factor in designing high- T_c superconducting electrides is that there is a high DOS occupation at E_f dominated by ISQ or host atoms, which determines its superconducting mechanism.

IV. CONCLUSIONS

The phase diagram of Li-C binary systems under high pressure up to 200 GPa was explored by using a combination of crystal-structure prediction and first-principles calculations. Eight stable lithium carbides are stabilized under pressure, among which Li_5C and Li_6C are electrides. In addition, $Cmcm-I$ Li_5C exhibits superconductivity with a maximum T_c of 5.7 K, which is attributed to EPC originating from the hybridization of host electrons. By contrast, Li_6C is an insulator under high pressure. Our predicted structures for Li_5C and Li_6C exclude the previously proposed high superconductivities (maximum of 48 K) estimated basing on energetically unfavorable structures, which highlights the necessity of performing thorough structure prediction in order to investigate accurately the physical properties of new materials.

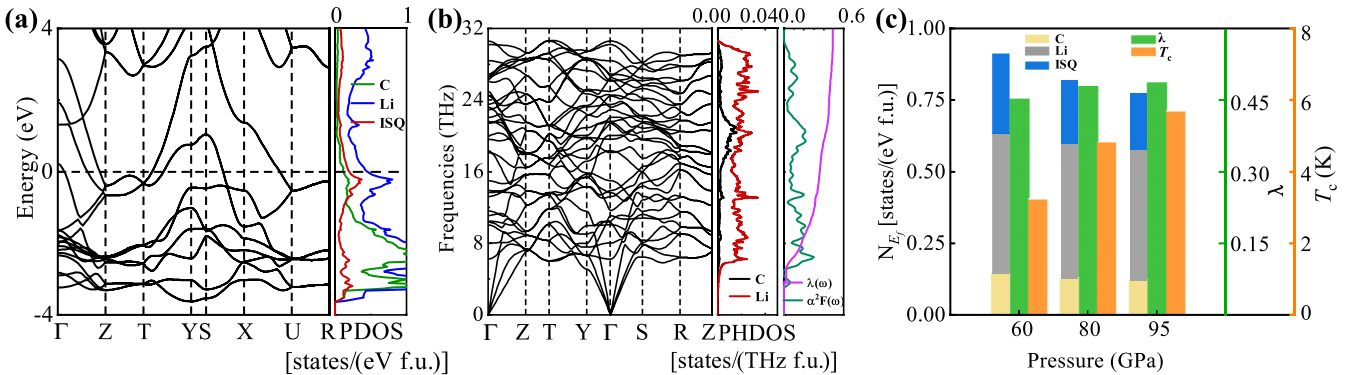


FIG. 4. (a) Calculated band structures and partial density of states (DOS), and (b) phonon dispersion and projected phonon DOS of $Cmcm-I$ at 95 GPa. (c) T_c , EPC parameter λ , and DOS of C, Li, and ISQs at the Fermi level (E_f) of $Cmcm-I$ at different pressures.

ACKNOWLEDGMENTS

The authors acknowledge funding from the NSFC under Grants No. 12074154, No. 11804128, No. 11722433, No. 12174160, and No. 11804129. Y.L. acknowledges the funding from the Six Talent Peaks Project and 333 High-level Talents Project of Jiangsu Province. J.H. acknowledges the

funding from the Science and Technology Project of Xuzhou under Grant No. KC19010. Q.W. acknowledges the founding from Postgraduate Research & Practice Innovation Program of Jiangsu Province No. 2021XKT1236. All the calculations were performed at the High Performance Computing Center of the School of Physics and Electronic Engineering of Jiangsu Normal University.

- [1] J. L. Dye, *Science* **301**, 607 (2003).
- [2] J. L. Dye, *Acc. Chem. Res.* **42**, 1564 (2009).
- [3] C. Liu, S. A. Nikolaev, W. Ren, and L. A. Burton, *J. Mater. Chem. C* **8**, 10551 (2020).
- [4] A. Ellaboudy, J. L. Dye, and P. B. Smith, *J. Am. Chem. Soc.* **105**, 6490 (1983).
- [5] S. Matsuishi, Y. Toda, M. Miyakawa, K. Hayashi, T. Kamiya, M. Hirano, I. Tanaka, and H. Hosono, *Science* **301**, 626 (2003).
- [6] M. Kitano, Y. Inoue, Y. Yamazaki, F. Hayashi, S. Kanbara, S. Matsuishi, T. Yokoyama, S.-W. Kim, M. Hara, and H. Hosono, *Nat. Chem.* **4**, 934 (2012).
- [7] K. Lee, S. W. Kim, Y. Toda, S. Matsuishi, and H. Hosono, *Nature (London)* **494**, 336 (2013).
- [8] J. Hu, B. Xu, S. A. Yang, S. Guan, C. Ouyang, and Y. Yao, *ACS Appl. Mater. Interfaces* **7**, 24016 (2015).
- [9] Y. Ma, M. Eremets, A. R. Oganov, Y. Xie, I. Trojan, S. Medvedev, A. O. Lyakhov, M. Valle, and V. Prakapenka, *Nature (London)* **458**, 182 (2009).
- [10] P. Chanhom, K. E. Fritz, L. A. Burton, J. Kloppenburg, Y. Filinchuk, A. Senyshyn, M. Wang, Z. Feng, N. Insin, J. Suntivich *et al.*, *J. Am. Chem. Soc.* **141**, 10595 (2019).
- [11] X. Zhang, Z. Xiao, H. Lei, Y. Toda, S. Matsuishi, T. Kamiya, S. Ueda, and H. Hosono, *Chem. Mater.* **26**, 6638 (2014).
- [12] Y. Zhang, H. Wang, Y. Wang, L. Zhang, and Y. Ma, *Phys. Rev. X* **7**, 011017 (2017).
- [13] Y. Li, Y. Wang, C. J. Pickard, R. J. Needs, Y. Wang, and Y. Ma, *Phys. Rev. Lett.* **114**, 125501 (2015).
- [14] H. Tang, B. Wan, B. Gao, Y. Muraba, Q. Qin, B. Yan, P. Chen, Q. Hu, D. Zhang, L. Wu *et al.*, *Adv. Sci.* **5**, 1800666 (2018).
- [15] A. R. Oganov, Y. Ma, Y. Xu, I. Errea, A. Bergara, and A. O. Lyakhov, *Proc. Natl. Acad. Sci. U.S.A.* **107**, 7646 (2010).
- [16] Y. Yao, J. S. Tse, and D. D. Klug, *Phys. Rev. Lett.* **102**, 115503 (2009).
- [17] M. Miyakawa, S. W. Kim, M. Hirano, Y. Kohama, H. Kawaji, T. Atake, H. Ikegami, K. Kono, and H. Hosono, *J. Am. Chem. Soc.* **129**, 7270 (2007).
- [18] Y. Zhang, B. Wang, Z. Xiao, Y. Lu, T. Kamiya, Y. Uwatoko, H. Kageyama, and H. Hosono, *npj Quantum Mater.* **2**, 1 (2017).
- [19] B. Lv, X. Y. Zhu, B. Lorenz, F. Y. Wei, Y. Y. Xue, Z. P. Yin, G. Kotliar, and C. W. Chu, *Phys. Rev. B* **88**, 134520 (2013).
- [20] Y. Ma, A. R. Oganov, and Y. Xie, *Phys. Rev. B* **78**, 014102 (2008).
- [21] J. Botana, J. Brgoch, C. Hou, and M. Miao, *Inorg. Chem.* **55**, 9377 (2016).
- [22] C. Kokail, C. Heil, and L. Boeri, *Phys. Rev. B* **94**, 060502(R) (2016).
- [23] X. Dong, J. Hou, J. Kong, H. Cui, Y.-L. Li, A. R. Oganov, K. Li, H. Zheng, X.-F. Zhou, and H.-T. Wang, *Phys. Rev. B* **100**, 144104 (2019).
- [24] Z. Zhao, S. Zhang, T. Yu, H. Xu, A. Bergara, and G. Yang, *Phys. Rev. Lett.* **122**, 097002 (2019).
- [25] X. Zhang, F. Li, A. Bergara, and G. Yang, *Phys. Rev. B* **104**, 134505 (2021).
- [26] Y. Tsuji, P. L. Dasari, S. Elatresh, R. Hoffmann, and N. Ashcroft, *J. Am. Chem. Soc.* **138**, 14108 (2016).
- [27] X. Li, A. Hermann, F. Peng, J. Lv, Y. Wang, H. Wang, and Y. Ma, *Sci. Rep.* **5**, 16675 (2015).
- [28] J.-Y. You, B. Gu, G. Su, and Y. P. Feng, *J. Am. Chem. Soc.* **144**, 5527 (2022).
- [29] X. Zhang and G. Yang, *J. Phys. Chem. Lett.* **11**, 3841 (2020).
- [30] M.-S. Miao and R. Hoffmann, *Acc. Chem. Res.* **47**, 1311 (2014).
- [31] S. Tanaka, T. Kato, A. Miyake, T. Kagayama, K. Shimizu, S. W. Kim, S. Matsuishi, and H. Hosono, *J. Korean Phys. Soc.* **63**, 477 (2013).
- [32] X.-L. Wang, K. An, L. Cai, Z. Feng, S. E. Nagler, C. Daniel, K. J. Rhodes, A. D. Stoica, H. D. Skorpenske, C. Liang *et al.*, *Sci. Rep.* **2**, 747 (2012).
- [33] E. Hazrati, G. A. de Wijs, and G. Brocks, *Phys. Rev. B* **90**, 155448 (2014).
- [34] D. Benson, Y. Li, W. Luo, R. Ahuja, G. Svensson, and U. Häussermann, *Inorg. Chem.* **52**, 6402 (2013).
- [35] X. Dong, L. Wang, K. Li, H. Zheng, Y. Wang, Y. Meng, H. Shu, H.-k. Mao, S. Feng, and C. Jin, *J. Phys. Chem. C* **122**, 20506 (2018).
- [36] L. Wang, X. Dong, Y. Wang, H. Zheng, K. Li, X. Peng, H.-k. Mao, C. Jin, Y. Meng, M. Huang *et al.*, *J. Phys. Chem. Lett.* **8**, 4241 (2017).
- [37] I. Efthimiopoulos, D. E. Benson, S. Konar, J. Nylén, G. Svensson, U. Häussermann, S. Liebig, U. Ruschewitz, G. V. Vazhenin, I. Loa, M. Hanfland, and K. Syassen, *Phys. Rev. B* **92**, 064111 (2015).
- [38] Y. Lin, T. A. Strobel, and R. E. Cohen, *Phys. Rev. B* **92**, 214106 (2015).
- [39] X. Jin, X.-J. Chen, T. Cui, H.-k. Mao, H. Zhang, Q. Zhuang, K. Bao, D. Zhou, B. Liu, Q. Zhou *et al.*, *Proc. Natl. Acad. Sci. USA* **113**, 2366 (2016).
- [40] Z. S. Pereira, G. M. Faccin, and E. Z. da Silva, *J. Phys. Chem. C* **125**, 8899 (2021).
- [41] Z. Liu, Q. Zhuang, F. Tian, D. Duan, H. Song, Z. Zhang, F. Li, H. Li, D. Li, and T. Cui, *Phys. Rev. Lett.* **127**, 157002 (2021).
- [42] Y. Wang, J. Lv, L. Zhu, and Y. Ma, *Phys. Rev. B* **82**, 094116 (2010).
- [43] Y. Wang, J. Lv, L. Zhu, and Y. Ma, *Comput. Phys. Commun.* **183**, 2063 (2012).
- [44] B. Gao, P. Gao, S. Lu, J. Lv, Y. Wang, and Y. Ma, *Sci. Bull.* **64**, 301 (2019).
- [45] W. Cui and Y. Li, *Chin. Phys. B* **28**, 107104 (2019).

- [46] W. Cui, T. Bi, J. Shi, Y. Li, H. Liu, E. Zurek, and R. J. Hemley, *Phys. Rev. B* **101**, 134504 (2020).
- [47] J. Shi, W. Cui, J. Hao, M. Xu, X. Wang, and Y. Li, *Nat. Commun.* **11**, 1 (2020).
- [48] K. Gao, W. Cui, J. Chen, Q. Wang, J. Hao, J. Shi, C. Liu, S. Botti, M. A. L. Marques, and Y. Li, *Phys. Rev. B* **104**, 214511 (2021).
- [49] Y. Li, X. Feng, H. Liu, J. Hao, S. A. Redfern, W. Lei, D. Liu, and Y. Ma, *Nat. Commun.* **9**, 1 (2018).
- [50] G. Kresse and J. Furthmüller, *Phys. Rev. B* **54**, 11169 (1996).
- [51] J. P. Perdew, K. Burke, and M. Ernzerhof, *Phys. Rev. Lett.* **77**, 3865 (1996).
- [52] H. J. Monkhorst and J. D. Pack, *Phys. Rev. B* **13**, 5188 (1976).
- [53] A. V. Krukau, O. A. Vydrov, A. F. Izmaylov, and G. E. Scuseria, *J. Chem. Phys.* **125**, 224106 (2006).
- [54] J. Klimeš, D. R. Bowler, and A. Michaelides, *Phys. Rev. B* **83**, 195131 (2011).
- [55] K. Parlinski, Z. Q. Li, and Y. Kawazoe, *Phys. Rev. Lett.* **78**, 4063 (1997).
- [56] A. Togo, F. Oba, and I. Tanaka, *Phys. Rev. B* **78**, 134106 (2008).
- [57] P. Giannozzi, S. Baroni, N. Bonini, M. Calandra, R. Car, C. Cavazzoni, D. Ceresoli, G. L. Chiarotti, M. Cococcioni, I. Dabo *et al.*, *J. Phys.: Condens. Matter* **21**, 395502 (2009).
- [58] P. B. Allen and R. Dynes, *Phys. Rev. B* **12**, 905 (1975).
- [59] E. Lee and K. A. Persson, *Nano Lett.* **12**, 4624 (2012).
- [60] See Supplemental Material at <http://link.aps.org/supplemental/10.1103/PhysRevB.106.054519> for the relative enthalpy as a function of pressure for all the considered Li_xC_y compounds, crystal structures of other Li-C compounds, charge transfers, the electronic properties and phonon dispersions of other compounds at different pressures and structure information of all the compounds, etc.
- [61] Y. Ge, S. Guan, and Y. Liu, *New J. Phys.* **19**, 123020 (2017).
- [62] X. Zeng, S. Zhao, Z. Li, and J. Yang, *Phys. Rev. B* **98**, 155443 (2018).